

# DSU-net: Dense SegU-net for automatic head-and-neck tumor segmentation in MR images<sup>\*</sup>

Pin Tang<sup>a,1</sup>, Chen Zu<sup>b,2</sup>, Mei Hong<sup>a,3</sup>, Rui Yan<sup>c,4</sup>, Xingchen Peng<sup>d,5</sup>, Jianghong Xiao<sup>e,6</sup>, Xi Wu<sup>f,7</sup>, Jiliu Zhou<sup>f,8</sup>, Luping Zhou<sup>g,9</sup> and Yan Wang<sup>a,\*,10</sup>

<sup>a</sup>School of Computer Science, Sichuan University, Chengdu, China

<sup>b</sup>Risk Controlling Research Department, JD.com, Chengdu, China

<sup>c</sup>School of Computer Science, Zhejiang University of Technology, Hangzhou, China

<sup>d</sup>Department of Biotherapy, Cancer Center, West China Hospital, Sichuan University, Chengdu, China

<sup>e</sup>Department of Radiation Oncology, Cancer Center, West China Hospital, Sichuan University, Chengdu, China

<sup>f</sup>School of Computer Science, Chengdu University of Information Technology, Chengdu, China

<sup>g</sup>School of Electrical and Information Engineering, University of Sydney, Australia

## ARTICLE INFO

### Keywords:

Nasopharyngeal carcinoma  
Dense SegU-net  
Magnetic resonance images

## ABSTRACT

Precise and accurate segmentation of the most common head-and-neck tumor, nasopharyngeal carcinoma (NPC), in MRI sheds light on treatment and regulatory decisions making. However, the large variations in the lesion size and shape of NPC, boundary ambiguity, as well as the limited available annotated samples conspire NPC segmentation in MRI towards a challenging task. In this paper, we propose a Dense SegU-net (DSU-net) framework for automatic NPC segmentation in MRI. Our contribution is threefold. First, different from the traditional decoder in U-net using upconvolution for upsampling, we argue that the restoration from low resolution features to high resolution output should be capable of preserving information significant for precise boundary localization. Hence, we use unpooling to unsample and propose SegU-net. Second, to combat the potential vanishing-gradient problem, we introduce dense blocks which can facilitate feature propagation and reuse. Third, using only cross entropy (CE) as loss function may bring about troubles such as miss-prediction, therefore we propose to use a loss function comprised of both CE loss and Dice loss to train the network. Quantitative and qualitative comparisons are carried out extensively on in-house datasets, the experimental results show that our proposed architecture outperforms the existing state-of-the-art segmentation networks.

## 1. Introduction

Nasopharyngeal carcinoma (NPC) is the most common head and neck malignancy arising from the nasopharynx (Zhong, Huang, Tang, Liang, Deng and Zhang, 2019), which can be treated by surgery, chemotherapy or by radiotherapy. Tumor volume is supposed to be the most intuitive indicator of NPC progression, especially in radiotherapy. Thus, optimum imaging is crucial for staging and radiotherapy planning of nasopharyngeal carcinoma (Brennan, 2006). Magnetic resonance images (MRI) has been a dominant imaging modality for the evaluation of marrow infiltration of the skull base, owing to its better resolution than CT and PET when it comes to assessing parapharyngeal spaces and primary tumor (Chua, Wee, Hui and Chan, 2016). Doctors have a great desire for the accurate and precise delineation of NPC, which is vital in radiotherapy as well as follow-up evaluations. However, nasopharyngeal tumor boundaries are currently manually delineated by oncologist slice by slice, which is at high risk of suffering from several deficiencies. First, highly view- and skill-dependent as well as subjected to the operator's experience and expertise, intra- and inter-operator segmentations may be in large discrepancy. Second, due to the low speed of manual segmentation, oncologists and experts are often trapped by this time-consuming and tedious work, giving rise to trustless or even incorrect segmentation. Third, taking this incorrectness propagation along the diagnose into consideration, final treat-

<sup>\*</sup> This document is the results of the research project funded by the National Natural Science Foundation of China (NSFC61701324).

<sup>\*</sup>Corresponding author

✉ tang.pin@outlook.com (P. Tang); chen0zu@gmail.com (C. Zu); hongmei@scu.edu.cn (M. Hong); yanrui2006@gmail.com (R. Yan); pxx2014@scu.edu.cn (X. Peng); xiaojh86@foxmail.com (J. Xiao); wuxi@cuit.edu.cn (X. Wu); zhoujl@cuit.edu.cn (J. Zhou); luping.zhou@sydney.edu.au (L. Zhou); wangyanscu@hotmail.com (Y. Wang)

ORCID(s): 0000-0002-2777-4933 (P. Tang); 0000-0002-8843-8685 (Y. Wang)

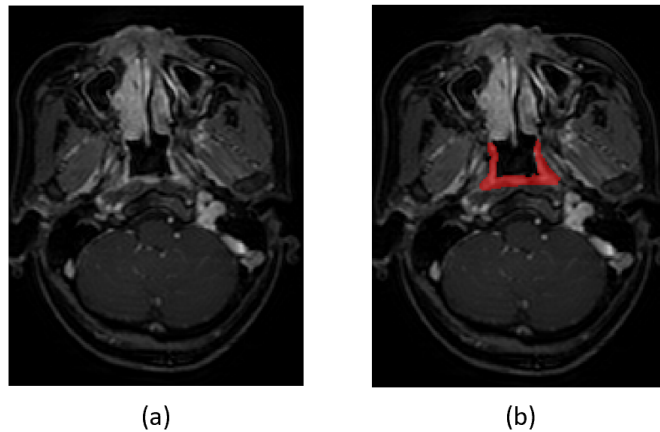


**Figure 1:** An example of (a) head-and-neck MR slice and its (b) manual segmentation of NPC

ment plans and decisions may be often biased probably. In this regard, automatic head-and-neck tumor segmentation methods in MRI are highly demanded to deliver efficient and accurate radiotherapy planning and follow-up assessment.

However, as shown in Fig. 1, NPC is adjacent to and even infiltrates into a few normal tissues such as mucosa that has almost the same intensity range as NPC (Ma, Wu, Song, Luo, Wang and Zhou, 2018). In addition, the lesion shape and size vary from patient to patient. Beyond that, the boundary ambiguity of head-and-neck tumors in MRI is also a sore point. As a result, an automatic approach for accurate and precise NPC segmentation remains to be challenging.

To cope with these problems, a large number of automatic NPC segmentation methods have been proposed previously. For example, Zhou, Chan, Xu and Chong (2006) developed a two-class support vector machine (SVM) based model to segment NPC from MRI. Tatanun, Ritthipravat, Bhongmakapat and Tuntiyatorn (2010) proposed a framework based on region growing method for NPC segmentation in CT images. Fitton, Cornelissen, Duppen, Steenbakkers, Peeters, Hoebbers, Kaanders, Nowak, Rasch and van Herk (2011) employed a semi-automatic and user-driven delineation algorithm named “snake” on weighted CT-MRI registered images. Huang, Zhao, Gong, Zha, Chen and Yang (2015) firstly calculated the NPC location adaptively and then utilized a hidden Markov random field model with maximum entropy for segmentation refinement.

The advent of deep learning is promising in resolving medical images related challenges (Wang, Zhou, Yu, Wang, Zu, Lalush, Lin, Wu, Zhou and Shen, 2018b; Wang, Yu, Wang, Zu, Lalush, Lin, Wu, Zhou, Shen and Zhou, 2018a). Unlike traditional machine learning methods which need to extract and choose features manually, deep learning methods like convolutional neural network (CNN) proposed by LeCun, Bottou, Bengio and Haffner (1998) and improved by Krizhevsky, Sutskever and Hinton (2012), have huge superiority in learning complex features automatically from the input. As a result, CNN has been widely applied to medical image segmentation. For instance, Tan, Fujita, Sivaprasad, Bhandary, Rao, Chua and Acharya (2017) applied a single CNN to automated segment exudates, haemorrhages, microaneurysms. Mao, Su, Xu, Wang, Huang, Yue, Sun and Xiong (2019) proposed a 4-D CNN for Attention-deficit/hyperactivity disorder (ADHD) fMRI classification. And Acharya, Fujita, Lih, Hagiwara, Tan and Adam (2017) try to detect arrhythmias using different intervals of tachycardia ECG segments with CNN.

Nevertheless, when using the traditional CNN trained in a sliding-window setup, the performance of the model is quite susceptible to the size of the selected image patches. Apart from this, traditional patch-based CNN models are obviously quite time-consuming for prediction since the network must be run individually for each patch. In addition, there is high and inevitable redundancy because of overlapping patches (Ronneberger, Fischer and Brox, 2015). With these issues in mind, end-to-end segmentation networks have attracted wide attention and reshaped the medical image segmentation field. In contrast to the networks based on image patches, the end-to-end networks such as fully convolutional networks (FCNs) take the whole image as the input and generate the output of the same size, so as to achieve the complete prediction results with only one forward calculation, which greatly saves the time overhead.

At present, a representative end-to-end network for medical image segmentation is U-net (Ronneberger et al., 2015), which is a typical encoder-decoder architecture named for its U-shaped symmetry structure. In U-net, Ronneberger et al. proposed a skip connection strategy which is based on concatenation, whose main idea is to merge the high

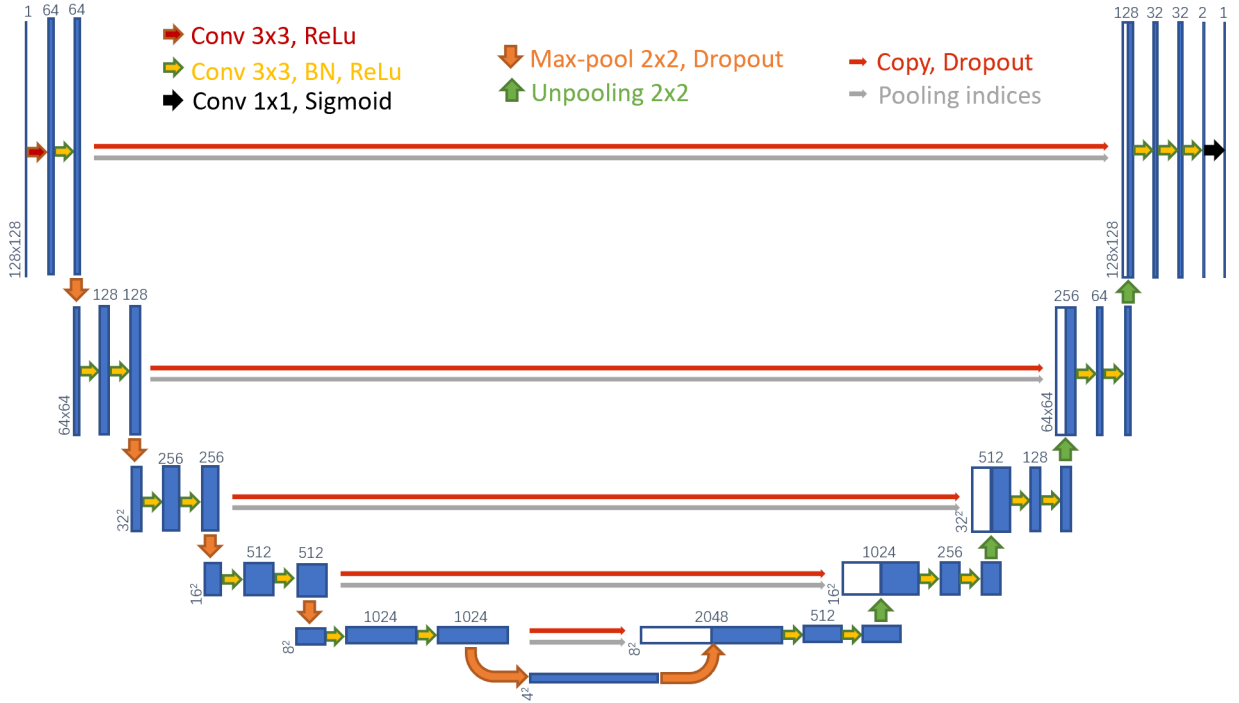


**Figure 2:** Schematic view of SegU-net. Blue boxes denote feature maps and white boxes denote copied feature maps from encoders. The number of feature maps and their x-y-size is respectively provided above the box and at the lower left edge of the box. The arrows represent the different operations

resolution features from the encoder in contracting path and the unsampled features from the corresponding decoder in expansive path, so that the feature information in the model can be effectively reused and the multi-level feature information in the model can be used jointly. The identical observation was obtained in another FCN based network (Nie, Wang, Gao and Shen, 2016), i.e., skip connection strategy can make full use of the features of the image and preserve boundary details, thus prominently improving the performance of the network.

U-net like architectures have now been widely used in many medical image segmentation tasks. Shenkman, Quteineh, Joskowicz, Szeskin, Yusef, Mayer and Eshed (2019) proposed an algorithm for automatic detection and diagnosis of sacroiliitis in CT, in which they use heuristics and a U-net classifier to compute the initial region of interest (ROI) that includes the pelvic joints region. Gupta, Kim, Vineberg and Balter (2019) applied a 3-channel U-net to generate synthetic CT images from MRI for treatment planning and patient positioning. Whereas, although U-net has remarkable performance on image processing and has been applied widely, when it is applied to NPC segmentation in MRI, it still cannot well handle the boundary ambiguity of NPC.

SegNet, which is proposed in (Badrinarayanan, Kendall and Cipolla, 2017), is another popular end-to-end network. In contrast to other models using upconvolution to unsample, SegNet proposed a simpler but more efficient unsampling method named unpooling, which can help to preserve the localization information. SegNet is also applied to semantic segmentation widely. For instance, Pradhan, Meyer, Vieth, Stallmach, Waldner, Schmitt, Popp and Bocklitz (2019) used SegNet to segment air tissue boundary in MRI. Tang, Li and Xu (2018) proposed a SegU-net method for gland Segmentation from colon cancer histology images.

In this paper, we focus on the problem of automatic NPC segmentation in MRI. With this purpose, as well as inspired by the appealing success achieved by U-net and motivated to tackle the thorny challenges faced by experts in clinical, we propose an automatic composite network named Dense SegU-Net (DSU-Net) to segment head-and-neck tumors from MRI. The contributions of our method are as follows. 1) Based on U-net, we first use unpooling introduced in SegNet to unsample and propose a segmentation network named as SegU-net to get over boundary ambiguity. 2) To alleviate the potential vanishing-gradient problem on account of the great increase of parameters, as well as facilitate feature propagation and reuse, we replace convolutional blocks with dense blocks and further propose

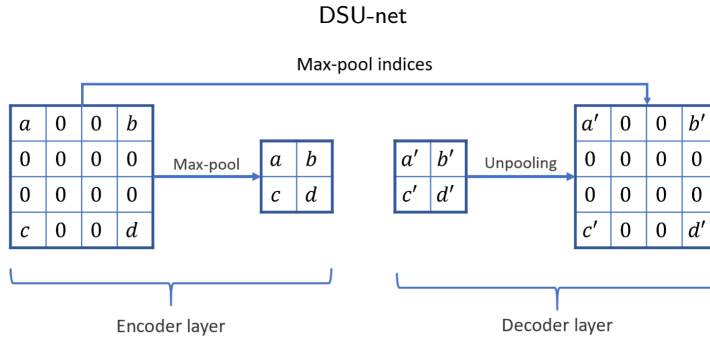


**Figure 3:** The principle of unpooling

a Dense SegU-net (DSU-net) that incorporates incorporate DenseNet (Huang, Liu, Van Der Maaten and Weinberger, 2017) and SegU-net. 3) To mitigate the potential problems on account of cross entropy (CE) loss, as well as to improve the performance of DSU-net, we use a composite loss function comprised of both CE loss and Dice loss in the training process of our model. 4) Compared with the other state-of-the-art networks, our method achieves better and higher performance, whilst incurring a fewer number of parameters and less computation.

## 2. Methodology

We first introduce the proposed SegU-net designed for NPC segmentation. Then we illustrate the entire encoder-decoder architecture, DSU-net, which aims at addressing potential problems caused by SegU-net. Details of these architectures together with the objective function are described in the following sections.

### 2.1. SegU-net

A schematic view of SegU-net is shown in Fig. 2. As an extension of U-net, SegU-net is also a U-shaped encoder-decoder structure. The feature-extraction component consists of a repeated block of two 3x3 convolutional layers with stride 1 and each block is followed by a 2x2 max pooling layer with stride 2. The number and size of feature channels will be doubled and halved respectively after successive convolution and max pooling operations for the sake of higher-level features learning and removal of local redundancy. Each decoder layer in the expansive path is composed of four parts: 1) a feature map concatenation block, which concatenates the feature maps after unpooling and the feature maps copied from the corresponding encoder layer; 2) a matrix consisting of max pooling indices passed by the encoder layer; 3) two 3x3 convolutions, each of which is followed by a batch normalization (BN) and Rectifier linear units (ReLU); 4) a 2x2 unpooling operation to upsample the feature maps so that the resolution of the images is increased.

Given that limited training data increases the risk of overfitting (Perez and Wang, 2017), a dropout (Srivastava, Hinton, Krizhevsky, Sutskever and Salakhutdinov, 2014) operation is introduced after each pooling operation and concatenation. It should be noted that the last convolutional block in the expansive path contains four convolutional layers, in which the first three convolutional layers have the identical structure and the last one is a 1x1 convolutional layer with stride 2, reducing the number of feature maps to 1. Afterward, the output is processed using the Sigmoid activation function such that each pixel value in the final output image drops in a range of 0 to 1, corresponding to the probability it belongs to the tumor area.

Compared with the traditional U-net based segmentation models, the innovation of the proposed SegU-net is that it adopts a new approach of upsampling named unpooling introduced in SegNet to replace upconvolution operation. The principle of unpooling is illustrated in Fig. 3. The indices of the max locations computed during pooling in the encoder layer are additionally saved and passed to the corresponding decoder layer. In the decoder, when the input feature maps are upsampled block by block to restore the image size, they are filled by zeros except for the maximum positions indicated by the saved indices, leading to sparse feature maps. As can be seen, implementing an upsampling operation in this way does not require learning. As demonstrated in (Yuan, Qin, Guo, Buyyounouski, Hancock, Han and Xing, 2019), the advantage of unpooling lies in which it can preserve some boundary details lost due to the consecutive down-sampling operations in encoder prominently. And these boundary details are of great importance for precise segmentation. Additionally, as an unsampling method, unpooling is an easier way compared with upconvolution since no parameters are required to learn.

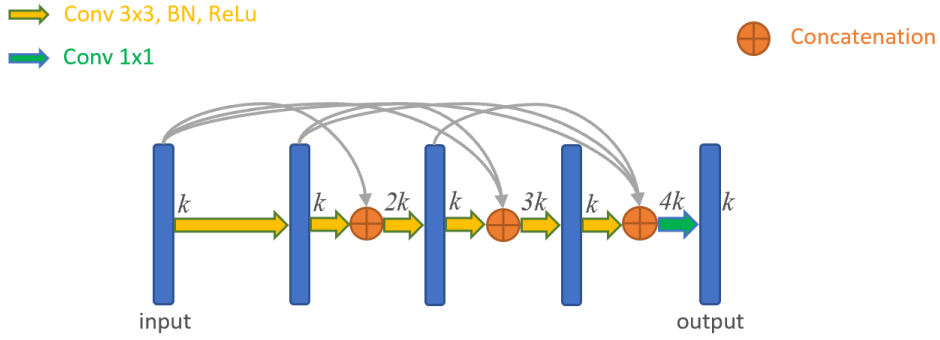


**Figure 4:** Structure of dense block adopted in this paper. Blue boxes represent feature maps. The arrows mean different operations.  $k$ ,  $2k$ ,  $3k$ , and  $4k$  above the yellow arrows denote the number of feature maps which the corresponding operation takes as input.

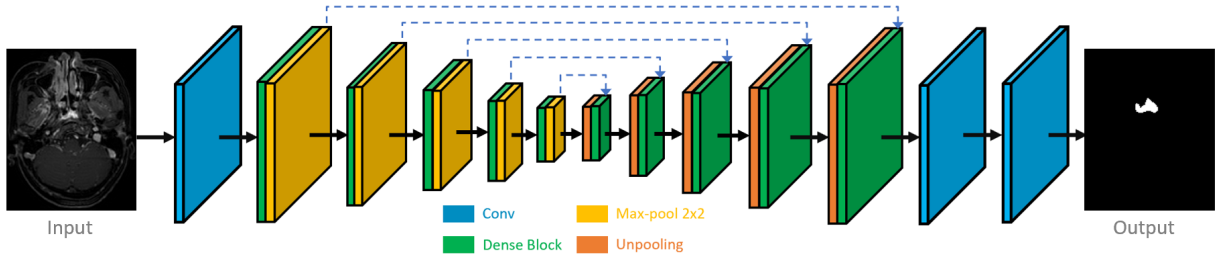


**Figure 5:** Architecture of Dense SegU-net. Blue boxes represent convolutional layers and green boxes represent dense blocks. The yellow boxes denote 2x2 max pooling while the orange boxes denote the unpooling operations. The black solid arrows denote convolutional operations and the blue dotted arrows are referred to the copy and concatenate operations as well as passing the pooling indices.

In order to reasonably utilize the unpooling operation while maintaining the original U-net structure as much as possible, an additional block containing only pooling and unpooling is added in SegU-net to separate the decoder and encoder of the network.

## 2.2. Dense SegU-net

The number of parameters and the time overhead of the proposed SegU-net is immense. Hence, overfitting and gradient-vanishing problem may adversely affect the learning process. In response to this situation, motivated by DenseNet, we further propose Dense SegU-net (DSU-net), in which we use dense blocks instead of convolutional blocks in the feature-extraction and the upsampling parts. Different from the general convolutional neural networks in which each convolutional layer only takes the feature maps from the previous one as its input, DenseNet concatenates feature maps learned by different layers, increasing variation in the input of subsequent layers in the dense block. Sharing feature maps with every other layer in a feed-forward fashion proves to be beneficial in considerably reducing the number of parameters to learn, encouraging feature reuse and alleviating the vanishing-gradient problem (Zeng and Xiao, 2019). As shown in Fig. 4, each dense block is composed of four convolutional layers. The first three use 3x3 kernels with stride 1 to extract features layer by layer. It is worth mentioning that we propose to utilize a 1x1 kernel at the end of each dense block to restrict the number of feature maps as the final output of dense block, so as to avoid the considerable increase of feature maps due to the deepening of the network. The BN and ReLu are applied after each convolution to simplify the training of deep neural networks. It is easy to calculate that the four convolutional layers take  $k$ ,  $2k$ ,  $3k$ , and  $4k$  feature maps as input, respectively, and the output of the dense block is a  $k$ -channel feature vector.

Based on the above dense blocks, the architecture of the proposed DSU-net is shown in Fig. 5. DSU-net still consists of the encoder part to analyze the input MRI slice and the decoder part to generate an output of segmented image. However, it replaces the convolutional blocks of SegU-net with dense blocks, and the number of dense blocks in

DSU-net is equal to the number of convolutional blocks in SegU-net, which is 10 totally. Meanwhile, the max-pooling and unpooling operations are remained the same between the dense blocks. In the encoder part of the model, a 3x3 convolutional layer with stride 1 is added to the front of the network to obtain  $k$  feature maps from the input image as the input of the first dense block, while in the decoder part, we add a 3x3 convolutional layer and a 1x1 convolutional layer with stride 1 to the last dense block to gain the final probability map.

### 2.3. Objective functions

In U-net, cross entropy (CE) loss function is employed in the training process and is defined as Equation 1.  $N$  is the total number of pixels in an MRI slice and  $i$  denotes the  $i^{th}$  pixel.  $y_t^i \in \{0, 1\}$  is the ground truth label of pixel  $x^i$ . Concretely, 0 refers to the normal tissues while 1 refers to the tumor that should be segmented.  $y_p^i$  ranges from 0 to 1 and represents the corresponding probability of  $x^i$  belonging to the tumor.

$$L_{CE} = -\frac{1}{N} \left( \sum_{i=1}^N y_t^i y_p^i + \sum_{i=1}^N (1 - y_t^i) (1 - y_p^i) \right) \quad (1)$$

As defined above, we can observe that different classes have the same contribution to the entropy loss. However, as shown in Fig. 1, the NPC tumor regions only account for a quite small part of the MRI slice. This unbalance of foreground and background makes the network prone to predict a pixel as background. Sun, Li, Liu, Zheng, Feng and Wang (2018) also has pointed out this problem. Additionally, some other researches (Mao, Li, Xie, Lau, Wang and Smolley, 2018; Shamsolmoali, Zareapoor, Wang, Jain and Yang, 2019) have proved that cross entropy loss may bring about gradient-vanishing problem. To handle these intractable issues, we introduce another prevailing loss function in semantic segmentation, Dice loss, in our segmentation network, which is defined as follows:

$$L_{Dice} = 1 - \frac{2 \sum_i^N y_p^i y_t^i + \epsilon}{\sum_i^N (y_p^i + y_t^i) + \epsilon} \quad (2)$$

where  $\epsilon$  represents a smooth term which is generally set to 1. The smooth term is quite necessary for numerical stability.

However, as reported in (Zhu, Huang, Zeng, Chen, Liu, Qian, Du, Fan and Xie, 2019), using the Dice loss only makes the optimization unstable especially in this unbalanced segmentation. Therefore, we propose to use a composite loss function that is comprised of both cross entropy loss and Dice loss as follows:

$$L = L_{Dice} + \lambda L_{CE} \quad (3)$$

where  $\lambda$  is a hyper-parameter to balance the two terms.

## 3. Experiments and results

### 3.1. Implementation details and datasets

We implemented both of our frameworks SegU-net and DSU-net with Pytorch. Model training and testing were conducted on an NVIDIA GeForce GTX 1080 Ti with 11GB memory using T1-weighted MRI of 95 NPC patients underwent chemoradiotherapy or radiotherapy at West China Hospital. Concretely, the MRI of 60 patients were selected as the training set, and the MRI of the other 15 patients as cross-validation samples, and the remaining 20 MRI of patients as test set. All the MRI were used with the approval of the radiology department of West China Hospital. These images have the same dimension of 160x275x103. Manual ground-truth annotation was provided by an experienced radiation oncologist on the MRI slice by slice.

It is noted that the acquired images are large scan volumes ranging from head to neck but the area occupied by the nasopharyngeal tumor is quite small in the MRI slice. For the sake of computational efficiency, as can be seen in Fig. 6, we first cropped the area with the size of 128x128 from the fixed position of each MRI slice as the region of interest (ROI), which is big enough to contain the whole possible tumor area. The cropped ROI is normalized to a range of 0 to 1 and used as the input in the subsequent training and testing process. In our experiment, a total of 1,628 MRI slices with the size of 128x128 were utilized as training set, and 374 as cross-validation set, 379 as test set, respectively.

Given that there are limited data samples available in the training set, to facilitate training, in this paper, the training set was additionally expanded by data augmentation methods including rotation, translation, and flip, as illustrated in

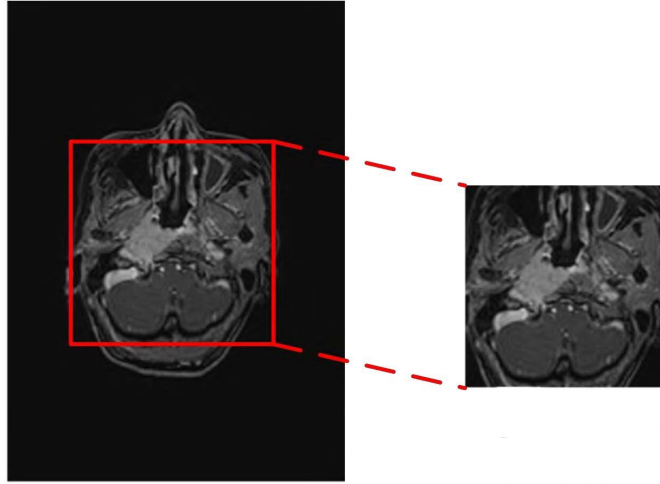


**Figure 6:** The extraction of region of interest. The image on the left is the original. The image after clip is shown on the right.

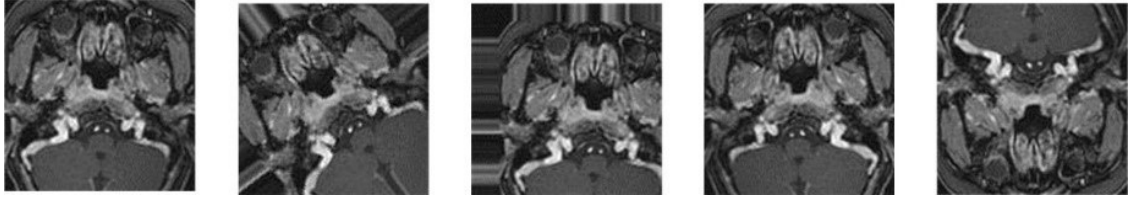


**Figure 7:** Data augmentation. From left to right, the original MR slice, the image after random rotation, the image after random translation, the image after horizontal flip and image after vertical flip.

Fig. 7. With these methods, the number of training samples was increased by five times the original number of samples, leading to 8,140 images finally acquired to train the network. Moreover, the network was trained by adaptive moment estimation (Adam) solver with mini-batch stochastic gradient descent (SGD). To be specific, the momentum term and the initial learning rate of Adam is 0.9 and 0.0001 respectively, and the mini-batch size is set to 32.  $\lambda$  is experimentally set to 1.

To ensure the performance of the model and rationality of the experimental results, the model with the minimum loss on the cross-validation set with minimum loss was selected as the final model to test on the samples in the test process.

### 3.2. Evaluation criteria

For segmentation evaluation, we assess the region and boundary similarities with four metrics, including dice similarity coefficient (DSC), prevent match (PM), correspondence ratio (CR), and average symmetric surface distance (ASSD). Let A and B denote the manual ground-truth and the automatically segmented slice, respectively.

The DSC is defined as the ratio between the size of the automatic segmented MRI slice intersecting the ground truth MRI slice, and the size of the automatic segmented MRI slice plus the ground truth MRI slice, which indicates the mutual overlap between segmentation and ground truth.

$$DSC = 2 \times \frac{|A \cap B|}{|A| + |B|} \quad (4)$$

According to this equation, it is easy to find that  $DSC = 1$  is referred to as an ideal segmentation while  $DSC = 0$  suggests that two segmentation have no overlaps. And according to the study of Zou et al., it can be identified as a good segmentation when the DSC value is greater than 0.7 (Zou, Warfield, Bharatha, Tempny, Kaus, Haker, Wells III, Jolesz and Kikinis, 2004).

Overlap-based metrics are generally not sensitive to the contour of segmentation, i.e., a high degree of segmentation overlaps does not mean the clinically relevant differences between their outlines are small enough to be ignored. On the contrary, those differences are what seriously matters for the target delineation in radiation therapy. Consequently, we employ a distance-based criterion called average symmetric surface distance (ASSD) as our evaluation metric. It is defined as:

$$ASSD = \frac{\sum_{a \in A} \min_{b \in B} d(a, b) + \sum_{b \in B} \min_{a \in A} d(b, a)}{|A| + |B|} \quad (5)$$

where  $d(a, b)$  denotes the Euclidean distance between  $a$  and  $b$ . It is obvious that a smaller ASSD value suggests a higher segmentation accuracy.

PM is the ratio of true positive (TP) to the number of tumor pixels in the ground truth. CR measures the correspondence of the segmentation result and the ground truth by weighting the importance of TP and false negative (FP). PM and CR can be employed to measure the over-segmentation and under-segmentation. They are formally defined as follows:

$$PM = \frac{TP}{GT} \quad (6)$$

$$CR = \frac{TP - 0.5 \times FP}{GT} \quad (7)$$

A greater value of PM and CR indicates less under-segmentation and less over-segmentation, respectively.

In conclusion, among the above four evaluation indicators, the larger the DSC, PM and CR and the smaller the ASSD, the better the segmentation performance, i.e., the closer the segmentation result is to the ground truth.

### 3.3. Quantitative and qualitative analysis

#### 3.3.1. The effectiveness of SegU-net

We first conduct our test experiment using SegU-net on MRI slices of 20 patients. Examples of segmentation results from four NPC patients are visualized in Fig. 8 and we can see that the segmentation results of SegU-net are very close to the ground truth.

Furthermore, we also compare the proposed SegU-net with SegNet and two types of U-net, one trained with only cross entropy loss (denoted as U-net(CE)) and another trained only with Dice loss (denoted as U-net(Dice)).

It can be seen from Table 1 that all these models have achieved good segmentation results when evaluating by DSC. Compared with the U-net trained with only cross entropy loss, the averaged DSC, PM, and CR of our method are increased by approximately 2.99%, 8.02%, 4.89%, respectively, and ASSD dropped by 0.0887. Compared with U-net trained with only Dice, the average DSC, PM, and CR of our method are increased by approximately 0.62%, 1.87%, 0.89%, respectively, and ASSD drops by 0.0639. Compared with SegNet, the averaged DSC, PM, and CR of SegU-net are increased by 3.94%, 6.32%, 5.77%, respectively, and ASSD drops by 0.1418. As can be seen, the proposed SegU-net presents more accurate and precise segmentation than U-net and SegNet in NPC segmentation. It is important to highlight that the U-net proposed in (Ronneberger et al., 2015) use only cross entropy loss to train the network. Another interesting finding is that, U-net can achieve better segmentation performance when trained with Dice loss than when trained with cross entropy loss since the mean DSC, PM, CR value of U-net with Dice loss are about 2.37%, 6.15%, 4% higher respectively while ASSD value drops about 0.024.

**Table 1**  
Quantitative comparison among SegNet, U-nets and SegU-net.

Method	DSC	PM	CR	ASSD(mm)
U-net(CE)	0.7654	0.7054	0.6405	0.9678
U-net(Dice)	0.7891	0.7669	0.6805	0.9440
SegNet	0.7559	0.7224	0.6317	1.0219
<b>SegU-net</b>	<b>0.7953</b>	<b>0.7856</b>	<b>0.6894</b>	<b>0.8801</b>

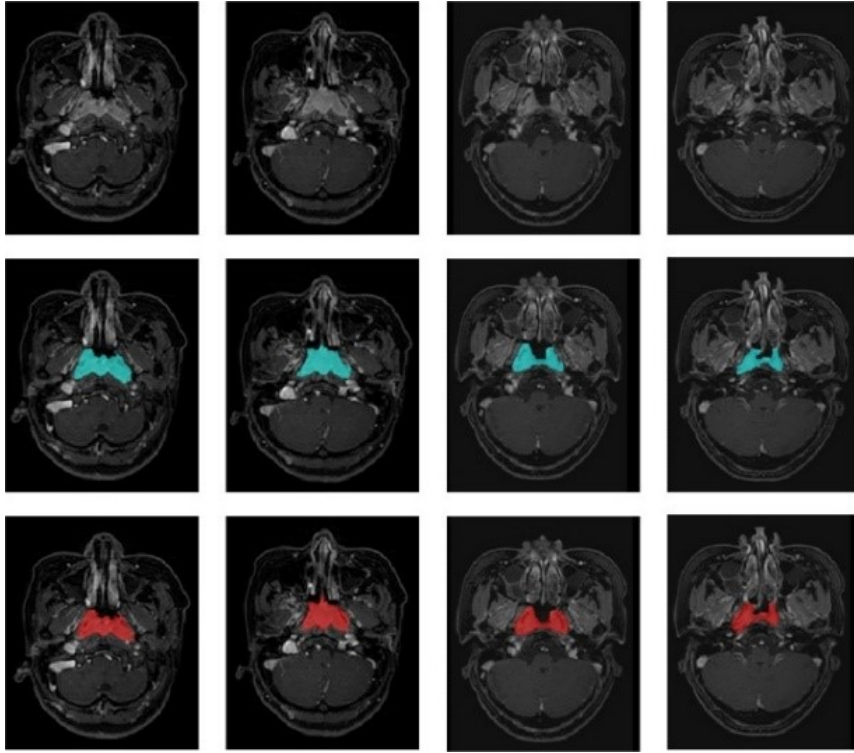


**Figure 8:** Visual segmentation results of SegU-net. Images in the first row are four examples of the test samples belonging to different patients. The second row shows the automatic segmentation results of SegU-net from the corresponding test samples given in the first row. The last row shows the ground truth.

### 3.3.2. Ablation study on unpooling and skip connection

We also conduct an ablation study to investigate the contribution factors of SegU-net to the segmentation performance improvement over U-net and SegNet, i.e., whether the improvement comes from the skip connection, unpooling operation, deepening the network or the increase number of feature maps. We conducted the experiment respectively use 1) SegU-net only employs skip connection in U-net, 2) SegU-net only employs unpooling, 3) the proposed SegU-net, i.e., with both skip connection and unpooling. The averaged quantitative comparison in terms of DSC, PM, CR, ASSD are provided in Table 2.

**Table 2**  
Quantitative comparion among SegNets.

Method	DSC	PM	CR	ASSD(mm)
SegU-net(only skip)	0.7903	<b>0.7869</b>	0.6833	0.9488
SegU-net(only unpooling)	0.7682	0.7373	0.6469	1.0414
<b>SegU-net</b>	<b>0.7953</b>	0.7856	<b>0.6894</b>	<b>0.8801</b>

Note that, compared with the SegU-net variant which removes the unpooling and the variant which removes the skip connection strategy, the SegU-net with both two strategies produces absolutely better performance on almost all the metric except PM. These results suggest that both skip connection and unpooling operation play vital roles and are indispensable to the superiority of SegU-net. However, the number of parameters has increased a lot, so further improvement is sensible and necessary.

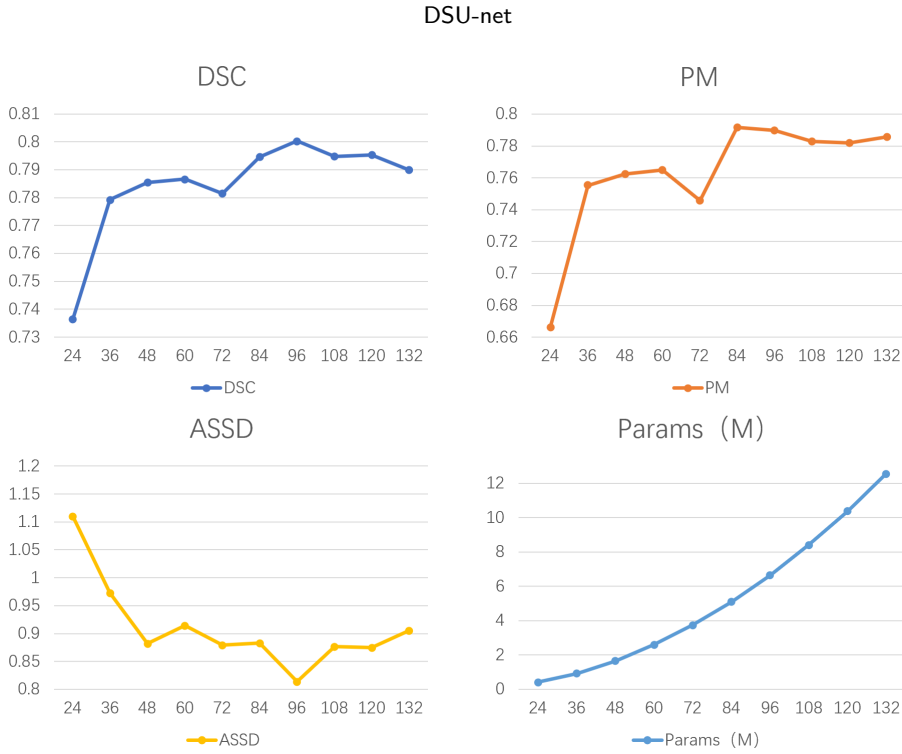


**Figure 9:** Qualitative comparison results of our DSU-net when  $k$  ranges from 24 to 132.

### 3.3.3. Impact of different values of $k$

As mentioned in Section 2.2, based on dense connection strategy, the size of  $k$  determines the number of feature maps that dense block takes as input and generates as output. Therefore, the value of  $k$  has significant impact on the performance of our proposed DSU-net. In Table 3 and Fig. 9, we compare the segmentation results of DSU-net with different  $k$  values. The evaluation metrics, including DSC and CR as well as the number of parameters (Params) gradually increase as  $k$  increases from 24 to 96, while ASSD gradually drops and the performance reaches the best when  $k$  is equal to 96. The value of PM is the highest when  $k$  equals 84. However, with the further increase of  $k$ , we found that the performance of DSU-net starts to decrease.

**Table 3**  
Qualitative comparison among different values of  $k$ .

$k$	DSC	PM	CR	ASSD(mm)	Params(M)
24	0.7364	0.6662	0.6037	1.1099	<b>0.41</b>
36	0.7793	0.7553	0.6668	0.9729	0.93
48	0.7854	0.7623	0.6773	0.8823	1.66
60	0.7866	0.7649	0.6773	0.9141	2.60
72	0.7815	0.7456	0.6679	0.8794	3.74
84	0.7945	<b>0.7917</b>	0.6913	0.8827	5.09
<b>96</b>	<b>0.8003</b>	0.7896	<b>0.6981</b>	<b>0.8136</b>	6.64
108	0.7948	0.7828	0.6901	0.8763	8.41
120	0.7953	0.7819	0.6909	0.8745	10.38
132	0.7899	0.7857	0.6848	0.9053	12.54

Consequently, we choose 96 as the value of  $k$  in DSU-net for NPC segmentation. We visualize segmentation results of our DSU-net when  $k = 96$  in Fig. 10, and we can observe that its segmentation is quite close to the ground truth. To intuitively show the improvement of our proposed model, the comparison results between SegU-net and DSU-net ( $k = 96$ ) are given in Table 4. We can see that the performance of DSU-net ( $k = 96$ ) is improved significantly. Apart

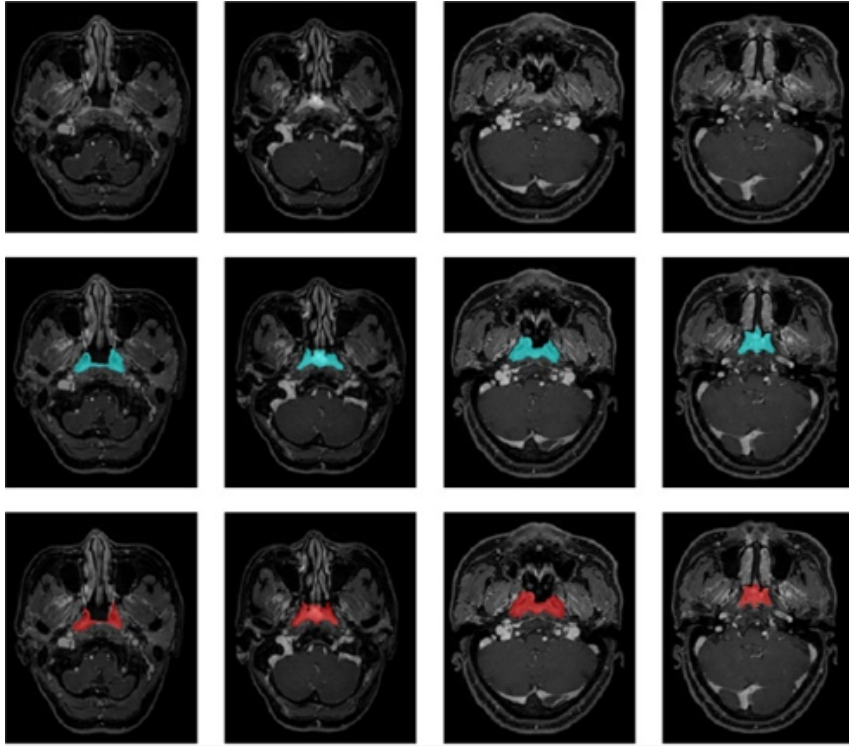


**Figure 10:** Visual segmentation results of DSU-net ( $k=96$ ). Images in the first row are the input slices. The second row shows the segmentation results of SegU-net. The last row is the ground truth.

from the evaluation metrics, it also remains necessary to simplify the structure of the network. As can be seen from Table 4, the number of parameters incurred by DSU-net is reduced by 80% compared with SegU-net, demonstrating that it is beneficial to replace the convolutional blocks with dense blocks.

**Table 4**

Quantative comparison between SegU-net and DSU-net when  $k = 96$ .

Method	DSC	PM	CR	ASSD(mm)	Params(M)
SegU-net	0.7953	0.7856	0.6894	0.8801	34.56
<b>DSU-net</b>	<b>0.8003</b>	<b>0.7896</b>	<b>0.6981</b>	<b>0.8136</b>	<b>6.64</b>

### 3.3.4. Comparison with the state-of-the-art methods

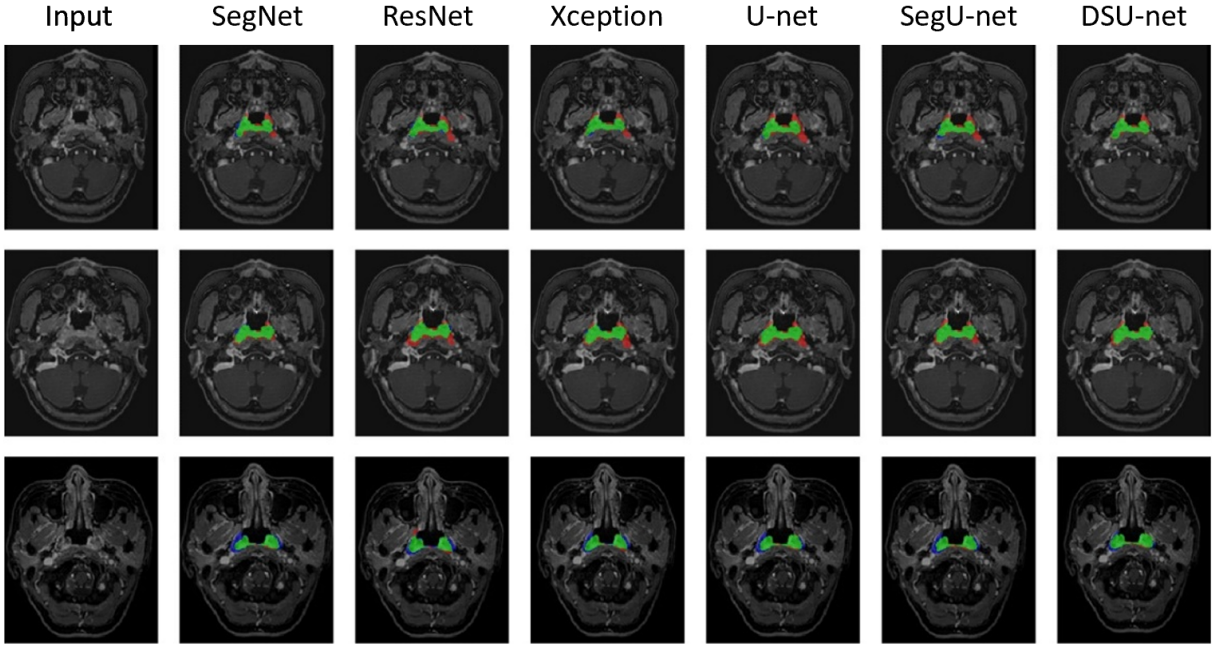
We compare our network with the state-of-the-art methods to evaluate the effectiveness of DSU-net, including SegNet, DeepLab (ResNet) (He, Zhang, Ren and Sun, 2016), DeepLab (Xception) (Chollet, 2017), and SegU-net. The quantitative evaluation results are provided in Table 5, from which we can see that all evaluation metrics of our proposed method show the best value, indicating that DSU-net achieves significant improvement and outperforms all the other methods in NPC segmentation.

Fig. 11 gives the visual comparison among the competitive networks mentioned above and our DSU-net. Through observation, we can intuitively see that DSU-net presents the most correct segmentation since the area occupied by green is the biggest while red and green only account for a little part compared with other methods. From these results, it can be concluded that our proposed DSU-net conquers the shortage of training samples, large lesion shape and size variation, as well as boundary ambiguity.

**Table 5**

Quantative comparison between state-of-the-art methods and DSU-net.

Method	DSC	PM	CR	ASSD(mm)
SegNet	0.7559	0.7224	0.6317	1.0219
DeepLab(ResNet)	0.7513	0.7361	0.6261	1.1671
DeepLab(Xception)	0.7638	0.7396	0.6408	1.1125
SegU-net	0.7953	0.7856	0.6894	0.8801
<b>DSU-net(<math>k=96</math>)</b>	<b>0.8003</b>	<b>0.7896</b>	<b>0.6981</b>	<b>0.8136</b>



**Figure 11:** Qualitative comparison of segmentation results with the state-of-the-art methods. From left to right, input image, SegNet, DeepLab (ResNet), DeepLab (Xception), U-net, SegU-net and Dense SegU-net. The green part represents the correct segmentation area, while the red part and blue part respectively represent the over-segmentation area and under-segmentation area.

## 4. Discussion

Deep learning based methods have been applied in many fields including medical image segmentation. However, the outline of head-and-neck tumors in MRI is still delineated by oncologists manually, which is quite time-consuming. Our work aims to provide an automatic approach to enhance the accuracy and expedite the progress of NPC segmentation. Although the idea of using U-net based model for segmentation has been proposed in the previous study (Nie et al., 2016; Dong, Yang, Liu, Mo and Guo, 2017), these methods use cross entropy loss in (Ronneberger et al., 2015), which has some drawbacks as stated in Section 2.3. Additionally, although skip connection offsets the lost boundary information in these methods, the contour of NPC still remains ambiguous which may be due to the nature of NPC such as large variations tumor size and shape, small intensity difference between normal issues and tumor and so on.

In this paper, we apply a composite loss to train our model to address these troubles and ease the training process. As for boundary information loss, we employ unpooling operation rather than upconvolution to further improve the accuracy of segmentation profile. From the experimental results in Section 3.3.1, we can see that SegU-net which adopted unpooling presents better segmentation than U-net, and the superiority of unpooling as a unsampling method is fully demonstrated.

The dense block proposed in (Huang et al., 2017) was first utilized in image classification but not in semantic

segmentation. However, the rationality of this application is supported by some related conclusions of recent researches (Bui, Shin and Moon, 2019; Wu, Li, Xiao, Geng, Zhang, Liu and Wang, 2019; Kumar Anand, Aurangabadkar, Khened and Krishnamurthi, 2019), i.e., the dense block has the ability to enhance feature propagation while well reduce the number of parameters. Experiments conducted in Section 3.3.3 and 3.3.4 exhibit the great performance and promising potential of our DSU-net.

Despite the great improvement mentioned above, there are still some limitations. First, the number of available training samples is limited at present. In future work, more MRI will be acquired to further enhance the generalization ability of our model. Second, 2D segmentation abandons the spatial information of the whole 3D MRI. However, spatial information plays a critical role in image segmentation and radiotherapy planning. Our future work will focus on developing 3D deep networks to take advantage of the 3D spatial information in medical images. Third, our current study focuses on NPC segmentation only in MRI. Nevertheless, every image modality has its own advantages and disadvantages and its own contributions to practice clinical treatment. So, it is also important to provide an automatic approach for multi-modality NPC segmentation.

## 5. Conclusion

In this work, we propose an outstanding network named Dense SegU-net for head-and-neck tumor segmentation in MRI, which would potentially promote NPC patient health monitoring and give crucial opportunities for accurate staging and radiotherapy planning of NPC. It can also significantly mitigate the burden on related experts and alleviate the differences among intra- and inter-operator. Different from the traditional image segmentation methods, we harness unpooling operation for its critical impact on boundary details reservation. Motivated by the success of Dense-net, we also employ the dense block in our network, which helps to achieve better performance while incurring a fewer number of additional parameters, and therefore overcoming the vanishing-gradient problem. Additionally, we propose to use a loss function comprised of cross entropy loss and Dice loss rather than use only cross entropy. The effectiveness of the proposed model is extensively verified by conducting comparison experiments with other competitive methods. However, there are still some possibilities remain to be explored. In the near future, more effort will be invested to improve the segmentation performance and we will investigate the potential of our network for general image semantic segmentation tasks.

## References

- Acharya, U.R., Fujita, H., Lih, O.S., Hagiwara, Y., Tan, J.H., Adam, M., 2017. Automated detection of arrhythmias using different intervals of tachycardia ecg segments with convolutional neural network. *Information sciences* 405, 81–90.
- Badrinarayanan, V., Kendall, A., Cipolla, R., 2017. Segnet: A deep convolutional encoder-decoder architecture for image segmentation. *IEEE transactions on pattern analysis and machine intelligence* 39, 2481–2495.
- Brennan, B., 2006. Nasopharyngeal carcinoma. *Orphanet Journal of Rare Diseases* 1, 23.
- Bui, T.D., Shin, J., Moon, T., 2019. Skip-connected 3d densenet for volumetric infant brain mri segmentation. *Biomedical Signal Processing and Control* 54, 101613.
- Chollet, F., 2017. Xception: Deep learning with depthwise separable convolutions, in: *Proceedings of the IEEE conference on computer vision and pattern recognition*, pp. 1251–1258.
- Chua, M.L., Wee, J.T., Hui, E.P., Chan, A.T., 2016. Nasopharyngeal carcinoma. *The Lancet* 387, 1012–1024.
- Dong, H., Yang, G., Liu, F., Mo, Y., Guo, Y., 2017. Automatic brain tumor detection and segmentation using u-net based fully convolutional networks, in: *annual conference on medical image understanding and analysis*, Springer. pp. 506–517.
- Fitton, I., Cornelissen, S., Duppen, J.C., Steenbakkers, R., Peeters, S., Hoebbers, F., Kaanders, J.H., Nowak, P., Rasch, C.R., van Herk, M., 2011. Semi-automatic delineation using weighted ct-mri registered images for radiotherapy of nasopharyngeal cancer. *Medical physics* 38, 4662–4666.
- Gupta, D., Kim, M., Vineberg, K.A., Balter, J.M., 2019. Generation of synthetic ct images from mri for treatment planning and patient positioning using a 3-channel u-net trained on sagittal images. *Frontiers in oncology* 9, 964.
- He, K., Zhang, X., Ren, S., Sun, J., 2016. Deep residual learning for image recognition, in: *Proceedings of the IEEE conference on computer vision and pattern recognition*, pp. 770–778.
- Huang, G., Liu, Z., Van Der Maaten, L., Weinberger, K.Q., 2017. Densely connected convolutional networks, in: *Proceedings of the IEEE conference on computer vision and pattern recognition*, pp. 4700–4708.
- Huang, K.W., Zhao, Z.Y., Gong, Q., Zha, J., Chen, L., Yang, R., 2015. Nasopharyngeal carcinoma segmentation via hmrf-em with maximum entropy, in: *2015 37th annual international conference of the IEEE engineering in medicine and biology society (EMBC)*, IEEE. pp. 2968–2972.
- Krizhevsky, A., Sutskever, I., Hinton, G.E., 2012. Imagenet classification with deep convolutional neural networks, in: *Advances in neural information processing systems*, pp. 1097–1105.
- Kumar Anand, V., Aurangabadkar, P., Khened, M., Krishnamurthi, G., 2019. Convolutional neural network for kidney and kidney tumor segmentation .

- LeCun, Y., Bottou, L., Bengio, Y., Haffner, P., 1998. Gradient-based learning applied to document recognition. *Proceedings of the IEEE* 86, 2278–2324.
- Ma, Z., Wu, X., Song, Q., Luo, Y., Wang, Y., Zhou, J., 2018. Automated nasopharyngeal carcinoma segmentation in magnetic resonance images by combination of convolutional neural networks and graph cut. *Experimental and therapeutic medicine* 16, 2511–2521.
- Mao, X., Li, Q., Xie, H., Lau, R.Y.K., Wang, Z., Smolley, S.P., 2018. On the effectiveness of least squares generative adversarial networks. *IEEE transactions on pattern analysis and machine intelligence*.
- Mao, Z., Su, Y., Xu, G., Wang, X., Huang, Y., Yue, W., Sun, L., Xiong, N., 2019. Spatio-temporal deep learning method for adhd fmri classification. *Information Sciences* 499, 1–11.
- Nie, D., Wang, L., Gao, Y., Shen, D., 2016. Fully convolutional networks for multi-modality isointense infant brain image segmentation, in: 2016 IEEE 13th international symposium on biomedical imaging (ISBI), IEEE. pp. 1342–1345.
- Perez, L., Wang, J., 2017. The effectiveness of data augmentation in image classification using deep learning. *arXiv preprint arXiv:1712.04621*.
- Pradhan, P., Meyer, T., Vieth, M., Stallmach, A., Waldner, M., Schmitt, M., Popp, J., Bocklitz, T., 2019. Semantic segmentation of non-linear multimodal images for disease grading of inflammatory bowel disease: A segnet-based application, in: *International Conference on Pattern Recognition Applications and Methods* 2019.
- Ronneberger, O., Fischer, P., Brox, T., 2015. U-net: Convolutional networks for biomedical image segmentation, in: *International Conference on Medical image computing and computer-assisted intervention*, Springer. pp. 234–241.
- Shamsolmoali, P., Zareapoor, M., Wang, R., Jain, D.K., Yang, J., 2019. G-ganlr: gradual generative adversarial network for image super resolution. *Neurocomputing* 366, 140–153.
- Shenkman, Y., Qutteineh, B., Joskowicz, L., Szeskin, A., Yusef, A., Mayer, A., Eshed, I., 2019. Automatic detection and diagnosis of sacroiliitis in ct scans as incidental findings. *Medical image analysis* 57, 165–175.
- Srivastava, N., Hinton, G., Krizhevsky, A., Sutskever, I., Salakhutdinov, R., 2014. Dropout: a simple way to prevent neural networks from overfitting. *The journal of machine learning research* 15, 1929–1958.
- Sun, H., Li, C., Liu, B., Zheng, H., Feng, D.D., Wang, S., 2018. Aunet: Attention-guided dense-upsampling networks for breast mass segmentation in whole mammograms. *arXiv preprint arXiv:1810.10151*.
- Tan, J.H., Fujita, H., Sivaprasad, S., Bhandary, S.V., Rao, A.K., Chua, K.C., Acharya, U.R., 2017. Automated segmentation of exudates, haemorrhages, microaneurysms using single convolutional neural network. *Information sciences* 420, 66–76.
- Tang, J., Li, J., Xu, X., 2018. Segnet-based gland segmentation from colon cancer histology images, in: 2018 33rd Youth Academic Annual Conference of Chinese Association of Automation (YAC), IEEE. pp. 1078–1082.
- Tatanun, C., Ritthipravat, P., Bhongmakapat, T., Tuntiyatorn, L., 2010. Automatic segmentation of nasopharyngeal carcinoma from ct images: Region growing based technique, in: 2010 2nd International Conference on Signal Processing Systems, IEEE. pp. V2–537.
- Wang, Y., Yu, B., Wang, L., Zu, C., Lalush, D.S., Lin, W., Wu, X., Zhou, J., Shen, D., Zhou, L., 2018a. 3d conditional generative adversarial networks for high-quality pet image estimation at low dose. *NeuroImage* 174, 550–562.
- Wang, Y., Zhou, L., Yu, B., Wang, L., Zu, C., Lalush, D.S., Lin, W., Wu, X., Zhou, J., Shen, D., 2018b. 3d auto-context-based locality adaptive multi-modality gans for pet synthesis. *IEEE transactions on medical imaging* 38, 1328–1339.
- Wu, J., Li, D., Xiao, Z., Geng, L., Zhang, F., Liu, Y., Wang, W., 2019. Retinal arteriosclerosis detection based on improved vgg-16 network. *Journal of Medical Imaging and Health Informatics* 9, 1892–1899.
- Yuan, Y., Qin, W., Guo, X., Buyyounouski, M., Hancock, S., Han, B., Xing, L., 2019. Prostate segmentation with encoder-decoder densely connected convolutional network (ed-densenet), in: 2019 IEEE 16th International Symposium on Biomedical Imaging (ISBI 2019), IEEE. pp. 434–437.
- Zeng, M., Xiao, N., 2019. Effective combination of densenet and bilstm for keyword spotting. *IEEE Access* 7, 10767–10775.
- Zhong, T., Huang, X., Tang, F., Liang, S., Deng, X., Zhang, Y., 2019. Boosting-based cascaded convolutional neural networks for the segmentation of ct organs-at-risk in nasopharyngeal carcinoma. *Medical physics* 46, 5602–5611.
- Zhou, J., Chan, K.L., Xu, P., Chong, V.F., 2006. Nasopharyngeal carcinoma lesion segmentation from mr images by support vector machine, in: 3rd IEEE International Symposium on Biomedical Imaging: Nano to Macro, 2006., IEEE. pp. 1364–1367.
- Zhu, W., Huang, Y., Zeng, L., Chen, X., Liu, Y., Qian, Z., Du, N., Fan, W., Xie, X., 2019. Anatomynet: Deep learning for fast and fully automated whole-volume segmentation of head and neck anatomy. *Medical physics* 46, 576–589.
- Zou, K.H., Warfield, S.K., Bharatha, A., Tempany, C.M., Kaus, M.R., Haker, S.J., Wells III, W.M., Jolesz, F.A., Kikinis, R., 2004. Statistical validation of image segmentation quality based on a spatial overlap index1: scientific reports. *Academic radiology* 11, 178–189.